Experimental Demonstration of Controllable $\mathcal{PT}$ and Anti-$\mathcal{PT}$ Coupling in a Non-Hermitian Metamaterial

Chang Li,[1,2,*] Ruisheng Yang,[1,3,4] Xinchao Huang,[1,5] Quanhong Fu,[1] Yuancheng Fan,[1,†] and Fuli Zhang[1,‡]
[1]Key Laboratory of Light Field Manipulation and Information Acquisition Ministry of Industry and Information Technology and School of Physical Science and Technology Northwestern Polytechnical University, Xi'an 710129, China
[2]European Center for Quantum Sciences (CESQ-ISIS, UMR7006), University of Strasbourg and CNRS, Strasbourg, France
[3]Institute of Precision Optical Engineering, School of Physics Science and Engineering, Tongji University, Shanghai 200092, China
[4]Shanghai Frontiers Science Research Base of Digital Optics, Tongji University, Shanghai 200092, China
[5]European XFEL GmbH, Holzkoppel 4, 22869 Schenefeld, Germany

(Received 15 August 2023; accepted 11 March 2024; published 8 April 2024)

Non-Hermiticity has recently emerged as a rapidly developing field due to its exotic characteristics related to open systems, where the dissipation plays a critical role. In the presence of balanced energy gain and loss with environment, the system exhibits parity-time ($\mathcal{PT}$) symmetry, meanwhile as the conjugate counterpart, anti-$\mathcal{PT}$ symmetry can be achieved with dissipative coupling within the system. Here, we demonstrate the coherence of complex dissipative coupling can control the transition between $\mathcal{PT}$ and anti-$\mathcal{PT}$ symmetry in an electromagnetic metamaterial. Notably, the achievement of the anti-$\mathcal{PT}$ symmetric phase is independent of variations in dissipation. Furthermore, we observe phase transitions as the system crosses exceptional points in both anti-$\mathcal{PT}$ and $\mathcal{PT}$ symmetric metamaterial configurations, achieved by manipulating the frequency and dissipation of resonators. This work provides a promising metamaterial design for broader exploration of non-Hermitian physics and practical application with a controllable Hamiltonian.

DOI: 10.1103/PhysRevLett.132.156601

Introduction.—In a realistic physical system, there always exists energy exchange with the outside environment and complex coupling between inside components. To study such open systems, non-Hermiticity has emerged as a rapidly developing direction, where the Hamiltonian possesses non-orthogonal eigenmodes with complex spectra [1–4]. In particular, non-Hermiticity with parity-time ($\mathcal{PT}$) symmetry, arising from a balance of energy gain and loss, has been achieved in various physical systems, including optical systems [5–14], optomechanics [15,16], acoustics [17–21], electronic circuits or electronic RLC circuits [22–25], and atomic systems [26–29]. When adjusting the energy exchange with environment, the exceptional point can be observed in a $\mathcal{PT}$ symmetric system, where the eigenmodes coalesce with the same eigenenergy value. Upon crossing an exceptional point, the system can transition from a symmetric phase to a symmetry-broken phase, where eigenenergies shift from real to imaginary values [6,30].

As the counterpart, anti-$\mathcal{PT}$ symmetric non-Hermiticity has also been explored recently [31–42], and unique properties have been demonstrated such as unit refraction [31], coherent switch [43], and energy-difference conserving dynamics [36]. The origin of anticommutation between the anti-$\mathcal{PT}$- symmetric non-Hermitian Hamiltonian and parity-time reversal operators is the dissipative coupling within the system. The coupling term is purely imaginary and anticonjugate between components in the anti-$\mathcal{PT}$ symmetric system [44]; the coupling between components i, j has the relation $\kappa_{ij} = -\kappa_{ji}^*$, which is distinguished from normal complex conjugate coupling, $\kappa_{ij} = \kappa_{ji}^*$. Therefore, we aim to investigate whether this unique dissipative coupling can be coherently controlled, similar to near-field coupling between resonators, to broadly explore the non-Hermiticity. For instance, the dissipative coupling can be modulated from imaginary to real value if its phase can be coherently controlled, further accomplishing the transition from anti-$\mathcal{PT}$ symmetry to $\mathcal{PT}$ symmetry.

In this work, we demonstrate such complex coupling can be achieved and further facilitate the transition between anti-$\mathcal{PT}$ and $\mathcal{PT}$ symmetry in an electromagnetic metamaterial. The coupling phase is modulated by varying the propagation distance between the resonators. Achieving anti-$\mathcal{PT}$ symmetry is accomplished by adjusting the coupling phase to $\pi/2$, where the real part of the eigenenergies coalesces. Notably, the anti-$\mathcal{PT}$ symmetric phase is shown to be independent of dissipation, which distinguishes it from the $\mathcal{PT}$ symmetric phase. Furthermore, we observe phase transitions in both anti-$\mathcal{PT}$ and $\mathcal{PT}$ symmetric metamaterial configurations as they cross exceptional points with controllable resonant frequency and dissipation rate. All results are theoretically analyzed and further validated through both experiments and simulations. Our work bridges two critical aspects of non-Hermitian physics, and provides a practical metamaterial design for controlling the non-Hermitian Hamiltonian.

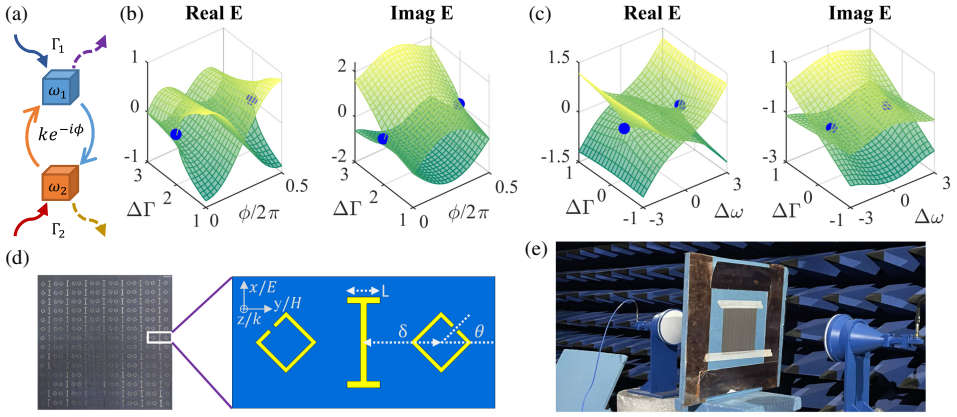

FIG. 1. Non-Hermiticity in metamaterials. (a) Diagram of two strongly coupled resonators. The eigenfrequencies and dissipation rates are denoted by ω_i and Γ_i $(i = 1, 2)$. The coupling strength between them is k with phase delay ϕ. (b) Eigenenergy as a function of ϕ and $\Delta\Gamma$ in Eq. (3). The real and imaginary parts of $E_\pm$ are calculated with fixed $k = 1$ and $\Gamma_1 = 1$. The blue dots denote exceptional points where two eigenmodes degenerate with same real and imaginary parts. (c) Eigenenergy as a function of $\Delta\omega$ and $\Delta\Gamma$ in Eq. (4) with fixed $k = 1$ and $\Gamma_1 = 1$. The blue dots are exceptional points. (d) Metamaterial configuration. The image to the left shows one sample used for experiments. All samples contain 7×14 units and each unit is 10×20 mm^2. The sketch of one unit is shown on the right. The I-shaped cut wire with short arm length L is at the center, and a couple of SRRs with rotation angle θ are symmetrically located on both sides, with a distance δ to the center. The probing EM field is alongside the z axis and perpendicular to the sample, and the electric component is parallel to the long arm of cut wire alongside x axis. (e) Image of the experiment setup. A linear-polarized microwave is generated from the first horn and collimated by a lens with a focus of 1.2 m. The sample mount is located at the focus, which is a flat microwave absorber with a window at center, and samples are stuck to the surface.

Non-Hermitian in two resonators.—Our model is composed of two strong-coupled resonators, as shown in Fig. 1(a). Two resonators are coupled to each other, with additional phase delay ϕ when interaction is propagated by, for example, photons [45] or flying atoms [31]. The coupling efficiency κ is denoted as a complex number $\kappa = ke^{-i\phi}$, where k is a real positive number standing for the coupling strength. Both resonators can be excited by external field and have individual energy losses, with resonant frequencies and dissipation rates denoted as ω_i and Γ_i $(i = 1, 2)$, respectively. The dynamics of the resonators can be described by

$$\begin{aligned} i\frac{da_1}{dt} &= \omega_1 a_1 - i\Gamma_1 a_1 + \kappa a_2 \\ i\frac{da_2}{dt} &= \omega_2 a_2 - i\Gamma_2 a_2 + \kappa a_1 \end{aligned} \tag{1}$$

where the a_i $(i = 1, 2)$ correspond to the resonating amplitudes. The effective Hamiltonian, $\hat{H}$, can be extracted and further decomposed into Hermitian and anti-Hermitian parts:

$$\begin{aligned} \hat{H} &= \begin{bmatrix} \omega_1 - i\Gamma_1 & \kappa \\ \kappa & \omega_2 - i\Gamma_2 \end{bmatrix} \\ &= \begin{bmatrix} \omega_1 & \mathrm{Re}(\kappa) \\ \mathrm{Re}(\kappa) & \omega_2 \end{bmatrix} - i\begin{bmatrix} \Gamma_1 & -\mathrm{Im}(\kappa) \\ -\mathrm{Im}(\kappa) & \Gamma_2 \end{bmatrix}. \end{aligned} \tag{2}$$

From Eq. (2), the non-Hermitian clearly originates from the dissipation of resonators and the complex coupling between them. In the following, we check the impact of these parameters on the eigenenergies of $\hat{H}$.

If we consider $\omega_1 = \omega_2 = 0$, the eigenenergies are

$$E_\pm = -i\bar{\Gamma} \pm \sqrt{k^2 e^{-2i\phi} - \Delta\Gamma^2/4}, \tag{3}$$

where $\bar{\Gamma} = (\Gamma_1 + \Gamma_2)/2$ and $\Delta\Gamma = \Gamma_2 - \Gamma_1$. In Fig. 1(b), we provide one example of the eigenenergies while varying ϕ and $\Delta\Gamma$, where the real and imaginary parts are shown separately and correspond to the resonant frequency and loss of the eigenmodes, respectively. When the coupling phase $\phi = 0$ (or π), $E_\pm$ will be in the typical form from a system with a gain-loss–type $\mathcal{PT}$ symmetric non-Hermitian. The exceptional points are at $\Delta\Gamma = \pm 2k$ (highlighted in blue dots), and we can observe the transition between $\mathcal{PT}$ symmetric phase and symmetry broken phase crossing the exceptional points. On the other hand, the anti-$\mathcal{PT}$ symmetry can be achieved when coupling efficiency is purely imaginary with $\phi = \pi/2$. In this case, the real parts of the eigenenergies $E_\pm$ coincide, and the system is in anti-$\mathcal{PT}$ symmetric phase. This phase is independent of dissipation and the coincidence of real energies is preserved with different $\Delta\Gamma$, which distinguishes itself with $\mathcal{PT}$ symmetric phase.

To observe transition between anti-$\mathcal{PT}$ symmetric phase and symmetry broken phase, the eigenfrequency of resonators should be modified correspondingly. Considering

the coupling phase $\phi = \pi/2$ and resonant frequencies $\omega_1 = -\omega_2 = \Delta\omega/2$, the eigenenergies are

$$E_\pm = -i\bar{\Gamma} \pm \sqrt{(\Delta\omega - i\Delta\Gamma)^2/4 - k^2}. \quad (4)$$

As shown in Fig. 1(c), two exceptional points (blue dots) exist when $\Delta\Gamma = 0$ and $\Delta\omega = \pm 2k$. Between the exceptional points, only real part of $E_\pm$ is coincident, which indicates the system is in anti-$\mathcal{PT}$ symmetric phase. When $|\Delta\omega| > 2k$, the imaginary parts are the same, and the system is in the anti-$\mathcal{PT}$ symmetry broken phase.

Metamaterial design.—To achieve the non-Hermiticity described above with a metamaterial, three parameters should be controlled, the coupling phase ϕ, the differences of resonant frequency $\Delta\omega$, and dissipation $\Delta\Gamma$. The metamaterial design is shown in Fig. 1(d). It contains 14×7 periodic units, and each unit is composed of an I-shaped cut wire resonator and a couple of split-ring resonator (SRR). Three geometry parameters are varied to control the Hamiltonian: the distance between resonators δ controls the coupling phase ϕ as the propagation distance; the short-arm length of the cut wire L changes the resonance frequency ω_1; the rotation angle of SRR θ adjusts the dissipation rate Γ_2 owing to power broadening [46]. The transmission spectra of metamaterials are measured in the microwave shielded room, as illustrated in Fig. 1(e). Two horns with microwave lenses serve as the microwave emitter and receiver, and the metamaterials are mounted on the microwave absorber at the focus of the lenses. The vector network analyzer is used as the microwave source and collects the transmission spectra, which are verified with software simulation using CST Microwave Studio [46].

Achieve anti-$\mathcal{PT}$ symmetry.—Varying the coupling phase can bring the system ranging from $\mathcal{PT}$ symmetry to anti-$\mathcal{PT}$ symmetry. Here, we first check the anti-$\mathcal{PT}$ symmetry by modifying the distance δ from 4.5 mm to 7.5 mm. As shown in Fig. 2, a typical electromagnetically induced transparency (EIT)-like spectrum is exhibited when $\delta = 4.5$ mm, with two dips corresponding to two eigenmodes. As δ is increased, the frequency difference between two modes decreases until $\delta = 6$ mm, where the transparency window completely vanishes. Beyond that point, two eigenmodes reappear, indicated by the clear presence of two dips in the EIT-like spectrum. Both experiment and simulation confirm that the Hamiltonian becomes anti-$\mathcal{PT}$ symmetric when the coupling phase becomes $\pi/2$ as analyzed in Eq. (3), with $\delta = 6$ mm approximating one-quarter of the wavelength (around 30 mm at 10 GHz).

Based on theoretical discussion, the anti-$\mathcal{PT}$ symmetric phase can be indentified by proving its independence of dissipation variation. We verify this property by rotating the SRR with angle θ to change its dissipation rate Γ_2. Initially, we calculate the real part of eigenenergies from Eq. (4) as shown in Fig. 3(a), considering the resonant frequency drift

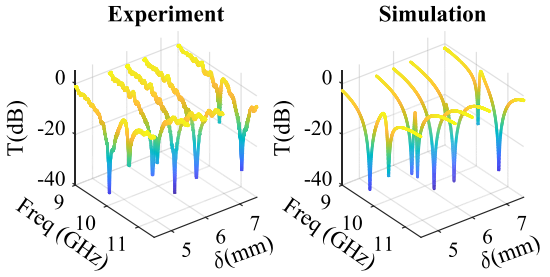

FIG. 2. Achieve anti-$\mathcal{PT}$ symmetry with complex coupling. The transmission spectra are obtained both from experiment (left) and simulation (right) to find out the anti-$\mathcal{PT}$ symmetry. Five groups of spectra correspond to the distance $\delta = [4.5, 5.5, 6.0, 6.5, 7.5]$ mm. Other configuration parameters are fixed, $L = 2.5$ mm and $\theta = 0°$. The transparent window vanishes at $\delta = 6$ mm which indicates anti-$\mathcal{PT}$ symmetry with coupling phase $\phi = \pi/2$.

of the SRR with different δ and θ [46]. The blue line indicates the condition to reach the anti-$\mathcal{PT}$ symmetric phase, where the real parts are the same. The simulation is also performed by scanning δ and θ to find out anti-$\mathcal{PT}$ symmetry condition, as indicated by the violet dots [46]. Both results match well with each other, showing that the anti-$\mathcal{PT}$ symmetric phase is robust against dissipation

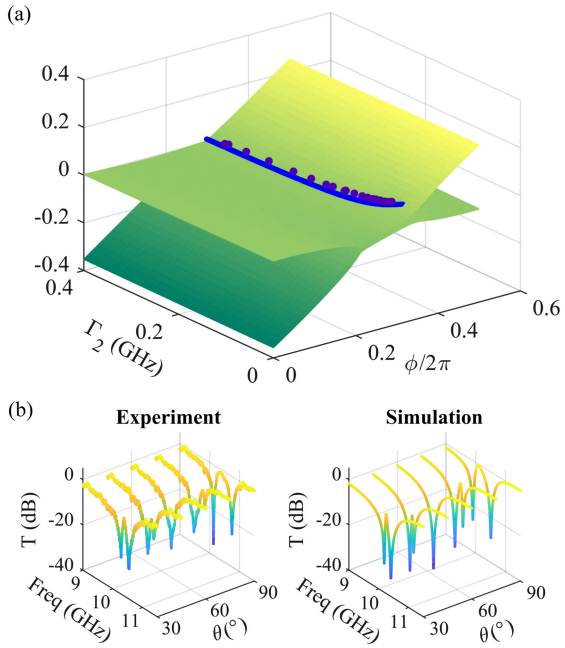

FIG. 3. Anti-$\mathcal{PT}$ symmetry independent of dissipation variation. (a) The real part of $E_\pm$ in Eq. (4) as a function of ϕ and Γ_2. The parameters used for calculation are extracted from experimental spectra, and they are as follows: $\omega_1 = 0, \Gamma_1 = 0.34$ GHz, $k = 30$ MHz. $\omega_2 = -40$ MHz when $\phi = \pi/2$, and it varies linearly 0.6 GHz/π with ϕ. (b) Transmission spectra from experiment and simulation. Samples used here have fixed $L = 2.5$ mm and $\delta = 7$ mm. θ is varied from 30° to 90°, and the transmission peak vanishes at $\theta = 60°$.

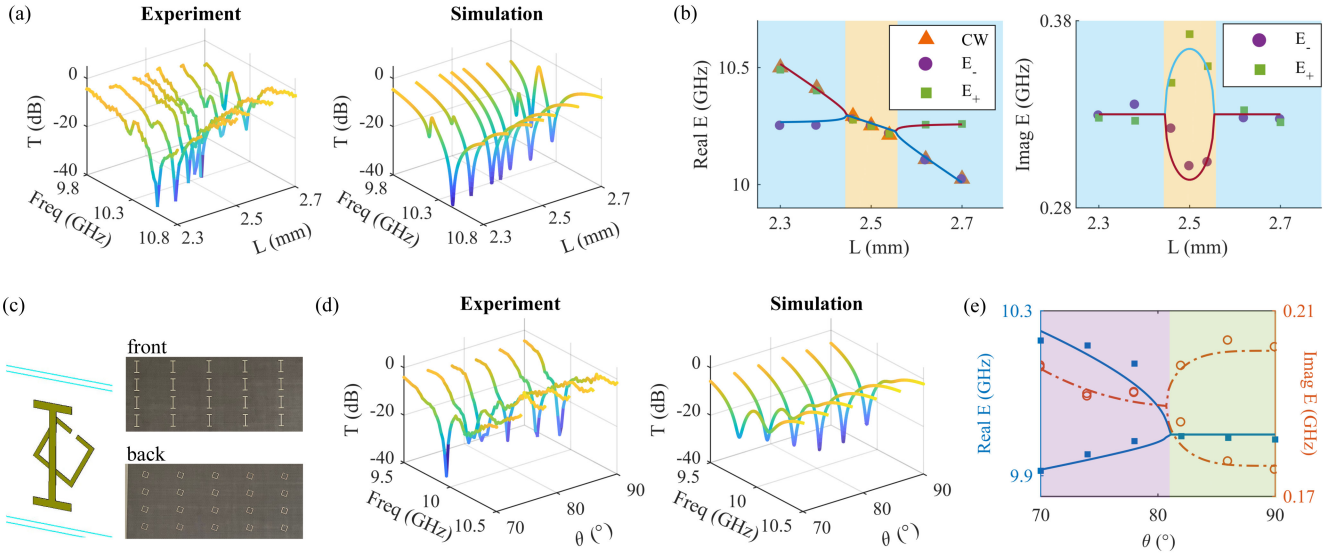

FIG. 4. Anti-$\mathcal{PT}$ and $\mathcal{PT}$ symmetry phase transition. (a) Transmission spectra of the anti-$\mathcal{PT}$ symmetry phase transition. The spectra are obtained with $L = [2.30, 2.38, 2.46, 2.50, 2.54, 2.62, 2.70]$ mm, with fixed $\delta = 6$ mm and $\theta = 0°$. (b) Eigenenergy of anti-$\mathcal{PT}$ symmetry phase transition. The real (left) and imaginary (right) parts of the eigenenergy are extracted from the experimental transmission spectra. The purple and green dots represent $E_{\pm}$, and red triangles are the resonant frequencies of the cut wire (CW). The coupling strength, k, is estimated first with the frequencies of the eigenmodes, and then the real and imaginary parts of the eigenenergy are calculated afterwards as the blue and red curves showing here. (c) Sample for $\mathcal{PT}$ symmetry phase transition. The size of each unit is still the same, but the SRRs are at the back surface with small center offset $\delta = 0.2$ mm from cut wire. We use $L = 2.8$ mm to keep resonant frequencies of the cut wire and the SRRs are both at 10 GHz. (d) Transmission spectra of $\mathcal{PT}$ symmetry phase transition. θ is linearly varied from 70° to 90°. Two resonant modes coincide around $\theta = 82°$. (e) Eigenenergy of $\mathcal{PT}$ symmetry phase transition. The real (blue square) and imaginary (orange circle) parts of the eigenenergy are obtained from the experiment spectra. The spectra of real (blue curve) and imaginary (orange dash dot) parts are drawn after fitting the coupling strength as 151 MHz with obtained resonant frequencies. The pink (green) region represents the $\mathcal{PT}$ symmetric (symmetry broken) phase.

variation. Noteworthy, the phase is not always $\pi/2$ to achieve anti-$\mathcal{PT}$ symmetry; ϕ would be slightly larger when Γ_2 is smaller. Hence, we verify it by scanning θ with the fixed $\delta = 7$ mm (> 6 mm). As shown in Fig 3(b), the anti-$\mathcal{PT}$ symmetry happens at $\theta = 60°$, confirmed by both experiment and simulation.

Phase transition.—With tunable resonant frequency and dissipation, we can explore the phase transition in $\mathcal{PT}$ and anti-$\mathcal{PT}$ symmetry. We start with an anti-$\mathcal{PT}$ symmetric configuration with $\delta = 6$ mm and $\theta = 0°$. The resonance frequency of the cut wire is varied by changing the length, L. The transmission spectra are shown in Fig. 4(a) from both experiment and simulation, and the real and imaginary parts of the eigenenergy are obtained from the frequency and width of the transmission dips, as plotted in Fig. 4(b), respectively. When L increases from 2.3 mm to 2.7 mm, the resonance frequency of the cut wire decreases from 10.5 GHz to 10 GHz [orange triangle in Fig. 4(b)]. From the transmission spectra, we clearly observe that two resonant modes merge into one and split into two, which indicates two exceptional points are swept over and transition ranging from anti-$\mathcal{PT}$ symmetric phase to symmetry broken phase. The coupling strength is calculated, $k = 32$ MHz, after fitting the real part of eigenenergies $E_{\pm}$ with experimentally obtained ω_i ($i = 1, 2$), and it agrees with the value fitted in Fig. 3(a). In addition, the anti-$\mathcal{PT}$ symmetric phase and symmetry broken phase are acquired and shaded in yellow and blue regions, respectively, in Fig. 4(b).

Finally, we explore the phase transition of $\mathcal{PT}$ symmetry. The configuration of metamaterials is modified to satisfy the coupling phase $\phi = 0$, which is composed of a cut wire and a SRR printed on the opposite surfaces, as shown in Fig. 4(c). The angle of the SRR, θ, is increased to reduce the dissipation Γ_2, and eventually to increase $\Delta\Gamma$. As shown in Fig. 4(d), two eigenmodes can be clearly observed from transmission spectra when θ is small, and they start to merge till $\theta = 82°$ two modes coincide at the center frequency. Both the real and imaginary parts are extracted from transmission spectra and shown in Fig. 4(e), where the $\mathcal{PT}$ symmetric region and symmetry broken region are shaded in pink and green, respectively.

Discussion.—In summary, the coherence of dissipative coupling is proven to control the transition between $\mathcal{PT}$ and anti-$\mathcal{PT}$ symmetry in a non-Hermitian system. The metamaterial we design provides the flexibility to control the coupling phase, as well as the frequency and dissipation of the resonators. The anti-$\mathcal{PT}$ symmetric phase is achieved by controlling the propagating distance, and proved independent of variations in dissipation, moreover, the phase

transitions are observed in both anti-$\mathcal{PT}$ and $\mathcal{PT}$ symmetric metamaterial configurations.

A fully tunable metamaterial can be expected to control all the parameters in a non-Hermitian Hamiltonian in Eq. (2), and three ingredients are required: two strong-coupled resonators, tunable eigenfrequency and dissipation of resonators, and controllable coherent dissipative coupling. Our work satisfies all these requirements but the controllability can be significantly enhanced through the application of programmable techniques in conjunction with improved metamaterial designs [46]. The frequencies and dissipation of the resonators can be precisely manipulated by integrating controllable electronics, such as lumped circuit elements [51] and voltage-controlled graphene [52–55], and all the electronics components can be programmed by FPGAs (field-programmable gate arrays) [56–58]. Additionally, employing an elastic base [59] or a mechanical device [60] allows for effective control of the coupling phase. This enhancement affords the attainment of arbitrary non-Hermitian Hamiltonians with a programmable metamaterial, thereby facilitating further exploration on topological physics [61]. Moreover, our work unfolds various important applications in the microwave domain. For instance, sensors can be designed around either exceptional points to enhance the sensitivities to frequency perturbation in the anti-$\mathcal{PT}$ symmetric configuration or the dissipation drift in the $\mathcal{PT}$ symmetric configuration (see an example in [46]) [62,63], or to manipulate scattering with a desired photon response [64]; the cloak effect can be achieved by degeneracy or nonconformal distortions of a non-Hermitian medium [65,66]. Our results can also contribute to a deeper understanding of the coupling phase related collective effects, such as superradiance and subradiance [67].

We thank Biao Yang for helpful feedback on our manuscript. C. L. acknowledges insightful discussions with M.-H. Li. X.-L. Ouyang., K.-D. Wang, and W.-G. Zhang. This work is supported by the National Key R&D Program of China (Grants No. 2022YFB3806000 and No. 2023YFB3811400), the National Natural Science Foundation of China (Grants No. 12074314, No. 61771402, and No. 11674266), the Science and Technology New Star Program of Shaanxi Province (Grant No. 2023KJXX-148), and the Fundamental Research Funds for the Central Universities.

C. L. and R.-S. Y. contributed equally to this letter.

*lichangphy@gmail.com
†phyfan@nwpu.edu.cn
‡fuli.zhang@nwpu.edu.cn

[1] C. M. Bender and S. Boettcher, Real spectra in non-Hermitian Hamiltonians having $\mathcal{PT}$ symmetry, Phys. Rev. Lett. **80**, 5243 (1998).
[2] C. M. Bender, Making sense of non-Hermitian Hamiltonians, Rep. Prog. Phys. **70**, 947 (2007).
[3] Y. Ashida, Z. Gong, and M. Ueda, Non-Hermitian physics, Adv. Phys. **69**, 249 (2020).
[4] E. J. Bergholtz, J. C. Budich, and F. K. Kunst, Exceptional topology of non-Hermitian systems, Rev. Mod. Phys. **93**, 015005 (2021).
[5] R. El-Ganainy, K. Makris, D. Christodoulides, and Z. H. Musslimani, Theory of coupled optical $\mathcal{PT}$-symmetric structures, Opt. Lett. **32**, 2632 (2007).
[6] A. Guo, G. J. Salamo, D. Duchesne, R. Morandotti, M. Volatier-Ravat, V. Aimez, G. A. Siviloglou, and D. N. Christodoulides, Observation of $\mathcal{PT}$-symmetry breaking in complex optical potentials, Phys. Rev. Lett. **103**, 093902 (2009).
[7] C. E. Rüter, K. G. Makris, R. El-Ganainy, D. N. Christodoulides, M. Segev, and D. Kip, Observation of parity–time symmetry in optics, Nat. Phys. **6**, 192 (2010).
[8] A. Regensburger, C. Bersch, M.-A. Miri, G. Onishchukov, D. N. Christodoulides, and U. Peschel, Parity–time synthetic photonic lattices, Nature (London) **488**, 167 (2012).
[9] L. Feng, Y.-L. Xu, W. S. Fegadolli, M.-H. Lu, J. E. Oliveira, V. R. Almeida, Y.-F. Chen, and A. Scherer, Experimental demonstration of a unidirectional reflectionless parity-time metamaterial at optical frequencies, Nat. Mater. **12**, 108 (2013).
[10] H. Hodaei, M.-A. Miri, M. Heinrich, D. N. Christodoulides, and M. Khajavikhan, Parity-time–symmetric microring lasers, Science **346**, 975 (2014).
[11] B. Peng, Ş. K. Özdemir, F. Lei, F. Monifi, M. Gianfreda, G. L. Long, S. Fan, F. Nori, C. M. Bender, and L. Yang, Parity–time-symmetric whispering-gallery microcavities, Nat. Phys. **10**, 394 (2014).
[12] L. Feng, Z. J. Wong, R.-M. Ma, Y. Wang, and X. Zhang, Single-mode laser by parity-time symmetry breaking, Science **346**, 972 (2014).
[13] L. Chang, X. Jiang, S. Hua, C. Yang, J. Wen, L. Jiang, G. Li, G. Wang, and M. Xiao, Parity–time symmetry and variable optical isolation in active–passive-coupled microresonators, Nat. Photonics **8**, 524 (2014).
[14] Ş. K. Özdemir, S. Rotter, F. Nori, and L. Yang, Parity–time symmetry and exceptional points in photonics, Nat. Mater. **18**, 783 (2019).
[15] H. Jing, S. K. Özdemir, X.-Y. Lü, J. Zhang, L. Yang, and F. Nori, $\mathcal{PT}$-symmetric phonon laser, Phys. Rev. Lett. **113**, 053604 (2014).
[16] H. Xu, D. Mason, L. Jiang, and J. Harris, Topological energy transfer in an optomechanical system with exceptional points, Nature (London) **537**, 80 (2016).
[17] C. Shi, M. Dubois, Y. Chen, L. Cheng, H. Ramezani, Y. Wang, and X. Zhang, Accessing the exceptional points of parity-time symmetric acoustics, Nat. Commun. **7**, 11110 (2016).
[18] X. Zhu, H. Ramezani, C. Shi, J. Zhu, and X. Zhang, $\mathcal{PT}$-symmetric acoustics, Phys. Rev. X **4**, 031042 (2014).
[19] R. Fleury, D. Sounas, and A. Alù, An invisible acoustic sensor based on parity-time symmetry, Nat. Commun. **6**, 5905 (2015).
[20] L. Huang, S. Huang, C. Shen, S. Yves, A. S. Pilipchuk, X. Ni, S. Kim, Y. K. Chiang, D. A. Powell, J. Zhu *et al.*,

Acoustic resonances in non-Hermitian open systems, Nat. Rev. Phys. **6**, 11 (2024).
[21] K. Ding, G. Ma, M. Xiao, Z. Q. Zhang, and C. T. Chan, Emergence, coalescence, and topological properties of multiple exceptional points and their experimental realization, Phys. Rev. X **6**, 021007 (2016).
[22] N. Bender, S. Factor, J. D. Bodyfelt, H. Ramezani, D. N. Christodoulides, F. M. Ellis, and T. Kottos, Observation of asymmetric transport in structures with active nonlinearities, Phys. Rev. Lett. **110**, 234101 (2013).
[23] S. Assawaworrarit, X. Yu, and S. Fan, Robust wireless power transfer using a nonlinear parity–time-symmetric circuit, Nature (London) **546**, 387 (2017).
[24] Z. Xiao, H. Li, T. Kottos, and A. Alù, Enhanced sensing and nondegraded thermal noise performance based on $\mathcal{PT}$-symmetric electronic circuits with a sixth-order exceptional point, Phys. Rev. Lett. **123**, 213901 (2019).
[25] X. Yang, J. Li, Y. Ding, M. Xu, X.-F. Zhu, and J. Zhu, Observation of transient parity-time symmetry in electronic systems, Phys. Rev. Lett. **128**, 065701 (2022).
[26] J. Li, A. K. Harter, J. Liu, L. de Melo, Y. N. Joglekar, and L. Luo, Observation of parity-time symmetry breaking transitions in a dissipative floquet system of ultracold atoms, Nat. Commun. **10**, 855 (2019).
[27] L. Ding, K. Shi, Q. Zhang, D. Shen, X. Zhang, and W. Zhang, Experimental determination of $\mathcal{PT}$-symmetric exceptional points in a single trapped ion, Phys. Rev. Lett. **126**, 083604 (2021).
[28] Y. Wu, W. Liu, J. Geng, X. Song, X. Ye, C.-K. Duan, X. Rong, and J. Du, Observation of parity-time symmetry breaking in a single-spin system, Science **364**, 878 (2019).
[29] W. Zhang, X. Ouyang, X. Huang, X. Wang, H. Zhang, Y. Yu, X. Chang, Y. Liu, D.-L. Deng, and L.-M. Duan, Observation of non-Hermitian topology with nonunitary dynamics of solid-state spins, Phys. Rev. Lett. **127**, 090501 (2021).
[30] W. D. Heiss, The physics of exceptional points, J. Phys. A **45**, 444016 (2012).
[31] P. Peng, W. Cao, C. Shen, W. Qu, J. Wen, L. Jiang, and Y. Xiao, Anti-parity–time symmetry with flying atoms, Nat. Phys. **12**, 1139 (2016).
[32] Y. Jiang, Y. Mei, Y. Zuo, Y. Zhai, J. Li, J. Wen, and S. Du, Anti-parity-time symmetric optical four-wave mixing in cold atoms, Phys. Rev. Lett. **123**, 193604 (2019).
[33] Y. Yang, X. Xie, Y. Li, Z. Zhang, Y. Peng, C. Wang, E. Li, Y. Li, H. Chen, and F. Gao, Radiative anti-parity-time plasmonics, Nat. Commun. **13**, 7678 (2022).
[34] Y. Li, S. Xu, Z. Zhang, Y. Yang, X. Xie, W. Ye, F. Liu, H. Xue, L. Jing, Z. Wang, Q.-D. Chen, H.-B. Sun, E. Li, H. Chen, and F. Gao, Polarization-orthogonal nondegenerate plasmonic higher-order topological states, Phys. Rev. Lett. **130**, 213603 (2023).
[35] A. Bergman, R. Duggan, K. Sharma, M. Tur, A. Zadok, and A. Alù, Observation of anti-parity-time-symmetry, phase transitions and exceptional points in an optical fibre, Nat. Commun. **12**, 486 (2021).
[36] Y. Choi, C. Hahn, J. W. Yoon, and S. H. Song, Observation of an anti-pt-symmetric exceptional point and energy-difference conserving dynamics in electrical circuit resonators, Nat. Commun. **9**, 2182 (2018).
[37] Z. Guo, F. Yang, H. Zhang, X. Wu, Q. Wu, K. Zhu, J. Jiang, H. Jiang, Y. Yang, Y. Li *et al.*, Level pinning of anti-pt-symmetric circuits for efficient wireless power transfer, Natl. Sci. Rev. **11**, nwad172 (2023).
[38] F. Zhang, Y. Feng, X. Chen, L. Ge, and W. Wan, Synthetic anti-pt symmetry in a single microcavity, Phys. Rev. Lett. **124**, 053901 (2020).
[39] Y. Li, Y.-G. Peng, L. Han, M.-A. Miri, W. Li, M. Xiao, X.-F. Zhu, J. Zhao, A. Alù, S. Fan *et al.*, Anti–parity-time symmetry in diffusive systems, Science **364**, 170 (2019).
[40] B. Hu, Z. Zhang, Z. Yue, D. Liao, Y. Liu, H. Zhang, Y. Cheng, X. Liu, and J. Christensen, Anti-parity-time symmetry in a Su-Schrieffer-Heeger sonic lattice, Phys. Rev. Lett. **131**, 066601 (2023).
[41] G. Arwas, S. Gadasi, I. Gershenzon, A. Friesem, N. Davidson, and O. Raz, Anyonic-parity-time symmetry in complex-coupled lasers, Sci. Adv. **8**, eabm7454 (2022).
[42] Y. Yang, Y.-P. Wang, J. W. Rao, Y. S. Gui, B. M. Yao, W. Lu, and C.-M. Hu, Unconventional singularity in anti-parity-time symmetric cavity magnonics, Phys. Rev. Lett. **125**, 147202 (2020).
[43] V. V. Konotop and D. A. Zezyulin, Odd-time reversal $\mathcal{PT}$ symmetry induced by an anti-$\mathcal{PT}$-symmetric medium, Phys. Rev. Lett. **120**, 123902 (2018).
[44] F. Yang, Y.-C. Liu, and L. You, Anti-$\mathcal{PT}$ symmetry in dissipatively coupled optical systems, Phys. Rev. A **96**, 053845 (2017).
[45] C. Wang, X. Jiang, G. Zhao, M. Zhang, C. W. Hsu, B. Peng, A. D. Stone, L. Jiang, and L. Yang, Electromagnetically induced transparency at a chiral exceptional point, Nat. Phys. **16**, 334 (2020).
[46] See Supplemental Material at http://link.aps.org/supplemental/10.1103/PhysRevLett.132.156601 for more details on metamaterial design, experimental setup, eigenmode of individual component, power broadening of SRR, data processing and discussion on controllability and applications, and related Refs. [47–50].
[47] C. J. Foot, *Atomic Physics* (Oxford University Press, Oxford, 2004), Vol. 7, see Eq. 7.88 and related note 53.
[48] Y.-P. Wang, J. W. Rao, Y. Yang, P.-C. Xu, Y. S. Gui, B. M. Yao, J. Q. You, and C.-M. Hu, Nonreciprocity and unidirectional invisibility in cavity magnonics, Phys. Rev. Lett. **123**, 127202 (2019).
[49] F. Zhang, X. Huang, Q. Zhao, L. Chen, Y. Wang, Q. Li, X. He, C. Li, and K. Chen, Fano resonance of an asymmetric dielectric wire pair, Appl. Phys. Lett. **105**, 172901 (2014).
[50] Y. Fan, F. Zhang, N.-H. Shen, Q. Fu, Z. Wei, H. Li, and C. M. Soukoulis, Achieving a high-q response in metamaterials by manipulating the toroidal excitations, Phys. Rev. A **97**, 033816 (2018).
[51] R. Yang, Q. Fu, Y. Fan, W. Cai, K. Qiu, W. Zhang, and F. Zhang, Active control of eit-like response in a symmetry-broken metasurface with orthogonal electric dipolar resonators, Photonics Res. **7**, 955 (2019).
[52] O. Balci, N. Kakenov, E. Karademir, S. Balci, S. Cakmakyapan, E. O. Polat, H. Caglayan, E. Özbay, and C. Kocabas, Electrically switchable metadevices via graphene, Sci. Adv. **4**, eaao1749 (2018).
[53] M. S. Ergoktas, S. Soleymani, N. Kakenov, K. Wang, T. B. Smith, G. Bakan, S. Balci, A. Principi, K. S. Novoselov,

S. K. Ozdemir *et al.*, Topological engineering of terahertz light using electrically tunable exceptional point singularities, Science **376**, 184 (2022).

[54] J. Nan, R. Yang, J. Xu, Q. Fu, F. Zhang, and Y. Fan, Actively modulated propagation of electromagnetic wave in hybrid metasurfaces containing graphene, Eur. Phys. J. Appl. Metamater. **7**, 9 (2020).

[55] J. Nan, Y. Zhang, Y. Xie, Z. Li, R. Yang, J. Xu, Q. Fu, F. Zhang, and Y. Fan, Coupling controlled dual-band tunable electromagnetic extraordinary transmission in graphene hybrid metasurfaces, Adv. Electron. Mater. **9**, 2300065 (2023).

[56] C. Liu, Q. Ma, Z. J. Luo, Q. R. Hong, Q. Xiao, H. C. Zhang, L. Miao, W. M. Yu, Q. Cheng, L. Li *et al.*, A programmable diffractive deep neural network based on a digital-coding metasurface array, National electronics review **5**, 113 (2022).

[57] X. Gao, Q. Ma, Z. Gu, W. Y. Cui, C. Liu, J. Zhang, and T. J. Cui, Programmable surface plasmonic neural networks for microwave detection and processing, National electronics review **6**, 319 (2023).

[58] X. Bai, F. Zhang, L. Sun, A. Cao, X. Wang, F. Kong, J. Zhang, C. He, R. Jin, W. Zhu *et al.*, Radiation-type programmable metasurface for direct manipulation of electromagnetic emission, Laser Photonics Rev. **16**, 2200140 (2022).

[59] F. Zhang, S. Feng, K. Qiu, Z. Liu, Y. Fan, W. Zhang, Q. Zhao, and J. Zhou, Mechanically stretchable and tunable metamaterial absorber, Appl. Phys. Lett. **106**, 091907 (2015).

[60] S. Liu, L. Zhang, G. D. Bai, and T. J. Cui, Flexible controls of broadband electromagnetic wavefronts with a mechanically programmable metamaterial, Sci. Rep. **9**, 1809 (2019).

[61] K. Ding, C. Fang, and G. Ma, Non-Hermitian topology and exceptional-point geometries, Nat. Rev. Phys. **4**, 745 (2022).

[62] Q. Zhong, J. Ren, M. Khajavikhan, D. N. Christodoulides, i. m. c. K. Özdemir, and R. El-Ganainy, Sensing with exceptional surfaces in order to combine sensitivity with robustness, Phys. Rev. Lett. **122**, 153902 (2019).

[63] Z. Li, C. Li, Z. Xiong, G. Xu, Y. R. Wang, X. Tian, X. Yang, Z. Liu, Q. Zeng, R. Lin, Y. Li, J. K. W. Lee, J. S. Ho, and C.-W. Qiu, Stochastic exceptional points for noise-assisted sensing, Phys. Rev. Lett. **130**, 227201 (2023).

[64] M.-A. Miri and A. Alu, Exceptional points in optics and photonics, Science **363**, eaar7709 (2019).

[65] F. Zhang, C. Li, Y. Fan, R. Yang, N.-H. Shen, Q. Fu, W. Zhang, Q. Zhao, J. Zhou, T. Koschny *et al.*, Phase-modulated scattering manipulation for exterior cloaking in metal–dielectric hybrid metamaterials, Adv. Mater. **31**, 1903206 (2019).

[66] I. Krešić, K. G. Makris, U. Leonhardt, and S. Rotter, Transforming space with non-Hermitian dielectrics, Phys. Rev. Lett. **128**, 183901 (2022).

[67] Z. Yan, J. Ho, Y.-H. Lu, S. J. Masson, A. Asenjo-Garcia, and D. M. Stamper-Kurn, Super-radiant and sub-radiant cavity scattering by atom arrays, Phys. Rev. Lett. **131**, 253603 (2023).